

ASME Journal of Biomechanical Engineering Online journal at:

https://asmedigitalcollection.asme.org/biomechanical



Gozde Basara

Department of Aerospace and Mechanical Engineering, University of Notre Dame, 225 Multidisciplinary Research Building, Notre Dame, IN 46556 e-mail: gbasara@nd.edu

Gokhan Bahcecioglu

Department of Aerospace and Mechanical Engineering, University of Notre Dame, 108B Multidisciplinary Research Building, Notre Dame, IN 46556 e-mail: gbahceci@nd.edu

Xiang Ren

Department of Aerospace and Mechanical Engineering, University of Notre Dame, Notre Dame, IN 46556 e-mail: xren@tju.edu.cn

Pinar Zorlutuna¹

Department of Aerospace and Mechanical Engineering, University of Notre Dame, Notre Dame, IN 46556; Department of Chemical and Biomolecular Engineering, University of Notre Dame, 143 Multidisciplinary Research Building, Notre Dame, IN 46556 e-mail: Pinar.Zorlutuna.1@nd.edu

An Experimental and Numerical Investigation of Cardiac Tissue-Patch Interrelation

Tissue engineered cardiac patches have great potential as a regenerative therapy for myocardial infarction. Yet, the mutual interaction of cardiac patches with healthy tissue has not been completely understood. Here, we investigated the impact of acellular and cellular patches on a beating two-dimensional (2D) cardiac cell layer, and the effect of the beating of this layer on the cells encapsulated in the patch. We cultured human-induced pluripotent stem cell-derived cardiomyocytes (iCMs) on a coverslip and placed gelatin methacryloyl hydrogel alone or with encapsulated iCMs to create acellular and cellular patches, respectively. When the acellular patch was placed on the cardiac cell layer, the beating characteristics and Ca⁺² handling properties reduced, whereas placing the cellular patch restored these characteristics. To better understand the effects of the cyclic contraction and relaxation induced by the beating cardiac cell layer on the patch placed on top of it, a simulation model was developed, and the calculated strain values were in agreement with the values measured experimentally. Moreover, this dynamic culture induced by the beating 2D iCM layer on the iCMs encapsulated in the cellular patch improved their beating velocity and frequency. Additionally, the encapsulated iCMs were observed to be coupled with the underlying beating 2D iCM layer. Overall, this study provides a detailed investigation on the mutual relationship of acellular/cellular patches with the beating 2D iCM layer, understanding of which would be valuable for developing more advanced cardiac patches. [DOI: 10.1115/1.4062736]

Keywords: cardiac patches, human-induced pluripotent stem cell-derived cardiomyocyte, gelatin methacryloyl, visible light crosslinking, finite element simulation

Introduction

Cardiovascular diseases (CVDs) have been the main cause of mortality worldwide [1,2]. Myocardial infarction (MI) is one of the most common CVDs and caused by the blockage of coronary arteries that leads to ischemia, and subsequent damage to the cardiac tissue. Having a limited capacity to regenerate, the damaged tissue is then replaced by resident fibroblasts and myofibroblasts, forming nonconductive scar tissue, ultimately leading to fatal arrhythmias [3,4].

Due to the specialized fibrillar structure, electrical conduction properties, and the limited healing capacity of the adult cardiac tissue, treatment of the damaged myocardium is one of the most challenging topics in regenerative medicine. Therefore, numerous studies are dedicated to developing methods to regenerate the myocardium such as injecting cells [5–7] or hydrogels [8,9], or placing cardiac patches on the damaged tissue [10]. Although cell

therapies have shown to improve the function of the heart, as well as reduce the scar size, injected cells often have low retention and survival rates [11]. Similarly, injecting hydrogels alone to the infarction site have shown to improve the cardiac function without causing an adverse immune response through supporting the ventricular wall [12]. Yet, there is still a need to find the injectable biomaterial that can support the coculture of cardiac cells [13]. Recently, cardiac patches have been the focus of many studies due to their therapeutic potential [14–16]. To develop the cardiac patches, a number of studies used biomaterials alone [17-20] whereas others incorporated cells, mainly stem cells [16] and human-induced pluripotent stem cell-derived cardiomyocytes (iCMs) [21,22], extracellular vesicles [23,24], and growth factors [25]. Various biomaterials [26] such as decellularized extracellular matrix (ECM) [10,27], collagen [15,17], gelatin methacryloyl (GelMA) [28,29], conductive polymers [30], and composites of hydrogels with conductive particles [31–34] have been used to engineer cardiac patches. Among these biomaterials, GelMA has been widely used in cardiac tissue engineering applications due to its tunable mechanical properties and cytocompatibility [28,29,35-37]. Even though cardiac patches have shown to improve the cardiac function,

¹Corresponding author.

Manuscript received November 21, 2022; final manuscript received June 6, 2023; published online June 21, 2023. Assoc. Editor: Joao S. Soares.

creating a smooth electrical integration between the cardiac patch and heart tissue [38] as well as the durability of the patch as it goes through cyclic contraction and relaxation are still remain as a challenge [39].

Current studies mostly assessed the therapeutic effect of the developed cardiac patches using animal models [15,40,41], by evaluating angiomyogenesis, scar tissue size, and cardiac functions [42]. While the effect of the patch on the heart tissue or cells was investigated in vivo [38], no study investigated how the cardiac patch influences the beating properties of the healthy tissue in vitro with human cells. Moreover, although it has been previously reported that when iCMs were injected into neonatal or infarcted adult hearts, they undergo maturation such as increased cell size [43,44], how the beating of the healthy tissue affects the maturity of the encapsulated iCMs in the patch is yet to be fully explored.

In our work, we investigated the impact of the acellular and cellular cardiac patches on the beating two-dimensional (2D) iCM layer underneath, as well as the effect of this beating layer on the cells encapsulated in the patch. First, we evaluated the effect of placing an acellular patch on the beating 2D iCM layer by analyzing cardiac-related protein expressions, beating, and Ca2+ transient properties. Then, we placed a cellular patch and investigated if the encapsulated iCMs improved the beating characteristics of the beating 2D iCM layer. Next, by developing a simulation model we analyzed the deformation of the patch caused by the cyclic contraction and relaxation of the beating 2D iCM layer. Finally, we investigated the effect of this dynamic cell culture model created by the cyclic motion of the beating 2D iCM layer on the encapsulated iCMs in the patch, through analyzing their shortterm (7 days) cardiac-related gene expressions, short-term (7 days) and long-term (21 days) protein expressions, beating, and Ca² handling characteristics. We observed that dynamic culture conditions slightly improved the beating characteristics of the encapsulated iCMs, yet the short-term (7 days) cardiac-related gene expressions remained unaffected. Moreover, we reported coupling between the encapsulated iCMs and the beating 2D iCM layer through Ca⁺² transient analysis. To the best of our knowledge, this is the first human in vitro study to investigate the mutual relationship between the beating iCM layer and the acellular or cellular cardiac patch, understanding which may be beneficial for developing better integrated cardiac patches.

Materials and Methods

hiPSC Culture and Human-Induced Pluripotent Stem Cell-Derived Cardiomyocytes Differentiation. DiPS 1016 SEVA hiPSC line derived from human skin (hiPSCs) were seeded in tissue culture flasks coated with Geltrex (1% Invitrogen, Carlsbad, CA) and maintained until 80% confluency using mTeSR (StemCell Technologies, Vancouver, BC, Canada) supplemented with 100 U/mL penicillin (Pen) (VWR, Radnor, PA). Then, they were detached using Accutase (StemCell Technologies), and seeded either in 12-well culture plates or on 12 mm diameter glass coverslips placed in 24-well culture plates in mTeSR1 media supplemented with Rhoassociated, coiled-coil containing protein kinase (ROCK) inhibitor (5 μ M, StemCell Technologies). Daily media changes were performed until 90% confluency was reached.

A previously established protocol was adapted to differentiate hiPSCs to iCMs [45]. Briefly, when the hiPSCs reached 90% confluency, they were treated with RPMI Medium 1640 (Life Technologies, Carlsbad, CA) supplemented with B27 without insulin (2% (w/v), Invitrogen), beta-mercaptoethanol (final concentration of 0.1 mM, Promega, Madison, WI), and Pen (100 U/mL) (CM (—)) with the addition of Wnt activator, CHIR99021 (CHIR) (10 µM, Stemgent, Cambridge, MA). Exactly 24 h later, the medium was replaced with CM (—) without CHIR. On day 4, CM (—) medium with the addition of Wnt inhibitor IWP-4 (5 µM, Stemgent) was used to treat the cells. On day 6, the medium was replaced with only CM (—). Three days later (day 9), medium was replaced with RPMI Medium 1640 supplemented with B27 (2%, Invitrogen),

beta-mercaptoethanol (final concentration of 0.1 mM, Promega), and Pen (100 U/mL) (CM (+)). After day 9, cells were maintained by media changes every 3 days, and beating was observed generally by day 21 of differentiation as previously reported [46,47].

Preparation of Patches. GelMA was synthesized by following the previously established protocol [48]. For the beating 2D iCM layer, hiPSCs were seeded on 12 mm glass coverslips, differentiated to iCMs as described in the previous section, and used between days 30 and 50. Acellular patches were prepared using GelMA and visible light photo-initiators (PIs) as follows: Visible light PI solution was prepared using Ruthenium (Ru) and Sodium Persulfate (SPS) following the manufacturer's instructions (Advanced Bio-Matrix). Simply, Ru and SPS were dissolved in phosphate-buffered saline (PBS) (Corning, Somerville, NY) (10 mM, pH 7.2) at 37.4 and 119 mg/mL concentrations, respectively. For the acellular patch, GelMA solution was prepared by dissolving GelMA (10% w/v) in PBS and Ru (2% w/v) and SPS (2% w/v) solutions were added.

To test the effect of placing an acellular patch on the beating iCM layer, a ring-shaped polydimethylsiloxane (PDMS) mold with a 7 mm inner diameter and 2 mm thickness was placed on the iCMs seeded on glass coverslips after removing the media. GelMA solution with Ru and SPS (17 μ l) was placed in the mold and immediately crosslinked using visible light (3 s). After crosslinking, the sample was washed with PBS and the PDMS mold was carefully removed using tweezers. The gels were then crosslinked further by treating them with microbial transglutaminase (mTGase, Modernist Pantry, Portsmouth, NH) solution (80 mg/mL w/v in CM+ media) at 37 °C for 30 min, which was refreshed after the first 15 min. The gels were then washed with CM+ media for another 15 min to ensure the removal of the PI from the gels. The patch-on-beating 2D iCM layer was maintained in culture in CM+ media with refreshing the media every 3 days.

To observe the effect of the cellular patch on the beating iCM layer, iCMs were mixed with GelMA solution prior to placing in the mold. For that, the GelMA solution was prepared as described above with double concentration. iCMs were collected using Trypsin ethylenediamine tetraacetic acid (EDTA) (VWR, Radnor, PA), resuspended in Dulbecco's Modification of Eagle's Medium (DMEM, Corning, Somerville, NY), supplemented with fetal bovine serum (FBS, 10%, Hyclone, Logan, UT), and penicillinstreptomycin (1%, Gibco, Waltham, MA) and then mixed with the GelMA solution at 1:1 ratio to have a final concentration of GelMA (10% w/v), Ru (2% w/v), SPS (2% w/v), and iCMs (40 million/mL).

Static and dynamic culture models were prepared to investigate the effect of beating 2D iCM layer on the encapsulated iCMs in the cellular patch. The static model was prepared by placing the cellular patch on the nonbeating iCM layer, and the dynamic culture was prepared by placing the cellular patch on the beating iCM layer, as described previously. The samples were kept for 7 days or 21 days in culture before doing any experiments with media changes every 3 days. All prepared conditions and corresponding abbreviations are summarized in Table 1.

Numerical Simulation. To study the effect of the contraction of the beating iCM layer on the gel deflection, a simple numerical model was created using COMSOL MULTIPHYSICS (version 4.4). Assuming the deformation of the hydrogel will stay in the elastic region, the linear elastic model was used [49]. The equations used for the linear elastic model are presented in Eqs. (1)–(3).

$$\rho \frac{\partial^2 u}{\partial t^2} - \nabla \cdot \sigma = F v, \quad \sigma = J^{-1} F S F^T, \quad F = (I + \nabla u), \quad J = \det(F)$$
(1)

$$S - S_0 = C : (\epsilon - \epsilon_0 - \epsilon_{inel})$$
 (2)

$$\epsilon = \frac{1}{2} \left[\left(\nabla \mathbf{u} \right)^T + \nabla \mathbf{u} + \left(\nabla \mathbf{u} \right)^T \nabla \mathbf{u} \right] \tag{3}$$

Table 1 Summary of prepared controls and conditions

Beating iCMs (BC)	Beating iCMs under acellular patch (BC-AP)	Cellular patch in static culture (CP-SC)	Cellular patch in dynamic culture (CP-DC)
Beating iCMs on glass	GelMA Beating iCMs on glass	GelMA + iCMs on glass	GelMA + iCMs iCMs on glass
Beating iCMs on glass cover slip	Acellular GelMA hydrogel is placed on top of beating iCMs layer on glass cover slip	iCMs encapsulated in GelMA hydrogel placed on non-beating iCMs layer on glass cover slip	iCMs encapsulated in GelMA hydrogel placed on beating iCMs layer on glass cover slip

The force applied by the beating iCM layer on the gel was measured experimentally using a nano-indenter (Optics 11, Amsterdam, The Netherlands), through dwell experiments as described previously [50,51]. Briefly, the nano-indenter probe (0.049 N/m spring constant, 3.5 μ m tip radius) was lowered down in the z direction until it touched the surface of the beating cell layer, and the beating cell layer was deflected $10 \, \mu m$. The probe was kept at that displacement for 30 s to record the deflection applied by the cells as they contracted. The contractile force of the cells is proportional to this deflection and was calculated using MATLAB (The MathWorks, Natick, MA) [51]. The beating cell layer on the glass coverslip and the gel on top of it were modeled using accurate dimensions (Fig. S1 of the Supplemental Materials on the ASME Digital Collection). Contact pair was defined between the bottom surface of the gel and the upper surface of the cells, and a thin elastic layer was defined for the contact pair. The contraction force that was experimentally measured was defined as a body load on the gel in the z direction. Fixed boundary condition was defined on the bottom surface of the glass cover slip. The material properties defined for the cells on glass cover and the gel are presented in Table 2.

Evaluation of the Effect of the Acellular and Cellular Patch on the Beating of the Two-Dimensional Human-Induced Pluripotent Stem Cell-Derived Cardiomyocytes Layer. To observe the effect of the acellular patch on the beating 2D iCM layer, acellular and cellular patches were prepared as described in the previous section. As a control, patch-free beating iCMs were used (Table 1). On day 7, phenotypical characterization, beating characterization was performed and Ca²⁺ handling properties were analyzed for patch-free beating iCMs and iCMs under the acellular patch. The details of each method are explained further in the following sections. To observe the effect of encapsulating iCMs in the patch on the beating performance of the underlying beating iCM layer, brightfield (BF) videos of the iCMs under the acellular and cellular patches were taken on day 7 and analyzed using an in-house MATLAB code. Additionally, Ca²⁺ staining was performed as described in detail in the following section.

Evaluation of the Effect of the Beating Two-Dimensional Human-Induced Pluripotent Stem Cell-Derived Cardiomyocytes Layer on the Human-Induced Pluripotent Stem Cell-Derived Cardiomyocytes Encapsulated in the Patch

Quantitative Real-Time Polymerase Chain Reaction. The shortterm effect of dynamic culture on the expression of cardiac-related

genes of the encapsulated iCMs was observed using the quantitative real-time polymerase chain reaction (qRT-PCR). The cellular patches were kept in either static or dynamic culture conditions for 7 days. On day 7, the iCMs encapsulated in the patches were collected. Briefly, gels were placed in liquid nitrogen and crushed using a tiny pestle and a mortar prior to mRNA isolation. Then, mRNA was collected using an mRNA isolation kit (RNeasy, Qiagen, Hilden, Germany) and its purity and concentration were measured using a Nano-Drop 2000 Spectrophotometer (Thermo Fisher Scientific, Waltham, MA). Afterward, cDNAs were synthesized, using the iScript cDNA Synthesis Kit (Bio-Rad, Hercules, CA). Certified human gene-specific primers were purchased from Bio-Rad, (Table S1 of the Supplemental Materials). iTaq SYBR Green Supermix (Bio-Rad) was used for qRT-PCR reactions, which were run in CFX Connect 96 Real-Time PCR system (Bio-Rad) in triplicates. The relative gene expression was plotted by applying the Δ Ct method using GAPDH as the housekeeping gene. $\Delta\Delta$ Ct method was used to calculate the fold changes between the cellular patches in dynamic culture (CP-DC) relative to static culture (CP-SC).

Transcriptome Analysis. Transcriptome analysis was performed using probe based Nano-String mRNA profiling. The mRNA isolation was performed following the same protocol described in the previous section. All samples were of sufficient quality for genomics analysis and were in duplicates. The gene expression levels were determined using Nanostring custom gene expression Panel (Nanostring Technologies, Seattle, WA). The data were normalized to the expression of iCMs cultured on tissue culture plastic as controls. Then all the counts were recalculated in log2 and the arithmetic means of log2 counts were taken as suggested by the Nanostring. Heat maps comparing the gene expressions were plotted using Graphpad software (San Diego, CA). The ratio between cellular patches in static and dynamic culture was considered to determine the most different gene counts.

Phenotypical Characterization. To investigate the short-term and long-term effects of the beating iCM layer on the encapsulated iCMs' sarcomere structure and Connexin 43 (CX43) expression, immunostaining was performed after 7 and 21 days in culture. At each time point, the cellular patches in static and dynamic cultures (n=3 for each) were washed with PBS (Corning) and fixed using paraformaldehyde (4%, Electron Microscopy Sciences, Hatfield, PA) for 45 min at room temperature. After fixing, three 10 min washes were done using PBS, and permeabilization was performed

Table 2 Material properties used for the numerical model

	Cells on glass coverslip	GelMA gel-acellular patch
Young's Modulus (kPa)	10 [82]	0.1 (Fig. S2 of the Supplemental Materials)
Poisson's ratio	0.45 [51]	0.45
Density (kg/m ³)	1055 [83]	1070 (calculated)

using Triton X-100 (0.1%, Sigma-Aldrich, St. Louis, MO) for 45 min. Then, the gels were washed with PBS thoroughly prior to blocking with goat serum (10%, Sigma-Aldrich) for 1 h. Sarcomeric alpha-actinin (SAA) (ab9465, Abcam, Cambridge, UK) and CX43 (ab11370, Abcam) primary antibody solutions were prepared in 10% goat serum at 1:200 and 1:100 dilutions, respectively. The gel samples were incubated in this solution at 4°C overnight. The next morning, the samples were washed thoroughly with PBS, before incubating in the secondary antibody solution (obtained by 1:200 dilution of Alexa Fluor 647 (A21245, Life Technologies) and Alexa Fluor 488 (A11001, Life Technologies) in goat serum) at 4 °C for 6 h. Before imaging, the samples were stained with DAPI (1:1000 dilution) (D9542, Sigma-Aldrich) and washed with PBS until no background was observed, then mounted using Pro-Long Gold antifade reagent (P36930, Thermo Fisher Scientific). Using a fluorescence microscope (Zeiss, Hamamatsu ORCA flash 4.0, Oberkochen, Germany), imaging was performed. The quantification for the sarcomere lengths and CX43 expression was performed using NIH IMAGEJ software.

Beating Characterization. The short-term and long-term effects of the dynamic culture on the beating performance of the encapsulated iCMs were investigated by using BF videos taken on day 7 and day 21. While taking the videos, the focus of the microscope was set to be on the encapsulated iCMs. The videos of the cellular patches in static and dynamic culture were analyzed using MATLAB adopting a block-matching algorithm to obtain beating velocity and beating frequency values as described previously [42].

Calcium (Ca²⁺) Handling and Synchronization Analysis. To assess the short-term and long-term effect of the dynamic culture on the contraction kinetics of the encapsulated iCMs, they were labeled using a Ca²⁺ sensitive dye and their Ca²⁺ handling properties were observed during the spontaneous beating. On day 7 (n = 3) and day 21 (n = 3) of culture (different samples were used), the medium was removed, and the samples were incubated in Fluo-4 AM solution (Thermo Fischer Scientific) at 37 °C for 30 min following manufacturer's instructions. Prior to imaging, the solution was replaced with warm CM (+) media that was previously removed from the cell culture well, and the imaging was performed immediately using a fluorescence microscope (Axio Observer Z1, Zeiss) at 200 ms exposure for 30 s. A customized MATLAB code was used to analyze the videos [31]. Briefly, the beating of the iCMs was identified using the green channel (calcium stain) of each frame, and the green intensities were normalized to the red channel of that frame. The intensity profile was then used to identify the time to peak, 50% decay time, and 90% decay time, where the maximum intensity point was identified as the peak. The Ca²⁺ transient properties of the cells were obtained by comparing the subsequent frames in each video in MATLAB. The red-green-blue (RGB) color images were analyzed individually, where red was used as the background and green was used as the beating profile. For the videos with weak fluorescence signals, the image was divided into 16 segments. The slice with the strongest beating profile was used as a representative beating profile for the specific video.

For the synchronization analysis, the Ca²⁺ flux videos were taken at the boundary of the underlying beating iCM layer and the cellular patch, while keeping the focus on the underlying beating iCM layer. The videos were then analyzed using a custom-made MATLAB code, as described previously [31]. Briefly, the video was divided into sixteen groups and the center of the beating of each group was identified. The Ca²⁺ transient profiles were plotted for each group considering the maximum intensity of the Ca²⁺ as the peak. Using the Ca²⁺ transient profiles of each group, the polar histograms were plotted considering the spontaneous Ca²⁺ transient as a periodic function, and the phase differences were measured in angular units as previously reported by our group [52].

Statistical Analysis. The results were reported as the mean- \pm standard deviation (SD) unless stated otherwise. For the Ca²⁺ flux experiments, 95% confidence interval was reported. The student's

t test was used to find any statistically significant differences and p < 0.05 was considered statistically significant.

Results

The Effect of Placing a Patch on the Beating Two-Dimensional Human-Induced Pluripotent Stem Cell-Derived Cardiomyocytes Layer

Acellular Patch. It is crucial to understand how the beating 2D iCM layer is affected when a patch is placed on top of it. An acellular patch was placed on the beating iCMs seeded on a glass coverslip, and the cells under the acellular patch (BC-AP) were compared to the patch-free beating cells (BC) on day 7, in terms of protein expression, beating and Ca⁺² handling properties. To observe the sarcomeric structure and cell-to-cell junctions, the cells were immunolabeled for SAA and CX43 (Fig. 1(a)). Both constructs expressed these proteins at comparable levels, yet when the average length of the sarcomeres was quantified, it was observed to be significantly longer for BC-AP (1.98 \pm 0.3 μ m) compared to BC $(1.84 \pm 0.3 \,\mu\text{m})$ (p = 0.0014), although the sarcomeres were not as organized (Fig. 1(b)). Moreover, the beating velocities were measured to be $6.7 \pm 3.5 \,\mu\text{m/s}$ and $3.8 \pm 0.5 \,\mu\text{m/s}$ and the frequencies to be $0.4 \pm 0.2\,\mathrm{Hz}$ and $0.3 \pm 0.1\,\mathrm{Hz}$ for BC and BC-AP, respectively (Figs. 1(c) and 1(d), indicating a significant decrease in the beating velocity (p = 0.001) after placing the patch on the iCMs. There was no significant difference between the beating frequencies. Finally, the Ca²⁺ transient profile of the BC and BC-AP was plotted using the Ca²⁺ flux intensity. Even though not significant, time to peak flux, 50% decay time, and 90% decay time values showed a decrease from $458.6 \pm 128.8 \,\mathrm{ms}$, $611.7 \pm 130.2 \,\mathrm{ms}$, and $802.5 \pm 136.0 \,\mathrm{ms}$ to $331.7 \pm 40.7 \,\mathrm{ms}$, $467.1.0 \pm 20.1 \,\text{ms}$, and $649.4 \pm 166.8 \,\text{ms}$, respectively, after placing the acellular patch on the underlying iCM layer (Fig. 1(e)).

Cellular Patch. The effect of iCMs encapsulated in the patch on the beating 2D iCM layer was evaluated by comparing the beating characteristics and Ca⁺² handling properties of the beating cells under an acellular patch (BC-AP) and beating cells under an iCMloaded, cellular patch (BC-CP) (Fig. 2). The beating velocity was higher for BC-CP $(7.2 \pm 3.8 \,\mu\text{m/s})$ compared to BC-AP $(4.9 \pm 1.3 \,\mu\text{m/s})$ (p = 0.0507) (Fig. 2(a)). Similarly, the beating frequency of BC-CP was higher (p = 0.0538) (1 \pm 0.6 Hz) compared to BC-AP $(0.7 \pm 0.5 \, \text{Hz})$ (Fig. 2(b)). When the effect of the encapsulated cells on the Ca²⁺ handling properties of the underlying beating cells was evaluated, the time to peak flux was measured to be 311.1 \pm 46.5 ms for BC-AP and 328.7 \pm 55.6 ms for BC-CP; the 50% decay time was $444.2 \pm 42.6 \,\mathrm{ms}$ for BC-AP and $503.0 \pm 62.9 \,\text{ms}$ for BC-CP; and the 90% decay time was $570.2 \pm 56.1 \,\text{ms}$ for BC-AP and $684.4 \pm 72.4 \,\text{ms}$ for BC-CP (Fig. 2(c)), indicating that the Ca⁺² handling properties of the beating 2D iCM layer were improved to the level of without any patches, in the presence of iCMs encapsulated in the patch.

The Effect of Beating Two-Dimensional Human-Induced Pluripotent Stem Cell-Derived Cardiomyocytes Layer on the Encapsulated Cells in the Cellular Patch

Numerical Simulation to Model the Cyclic Deformation of the Patch Caused by the Cardiac Cycle of the Beating Two-Dimensional Human-Induced Pluripotent Stem Cell-Derived Cardiomyocytes Layer. When the patch was placed on the beating 2D iCM layer, a macroscale deformation of the patch was observed (Video S1 of the Supplemental Materials on the ASME Digital Collection). To better understand this deformation exerted by the contraction of the beating 2D iCM layer on the acellular patch placed on top, a finite element model was developed. Using this model, the resultant displacement, strain, and stress exerted on the patch by the beating iCM layer were calculated (Fig. 3). When the underlying beating iCM layer was in a relaxation state, the total displacement on the gels was zero. During contraction, the total displacement was 850 μ m on

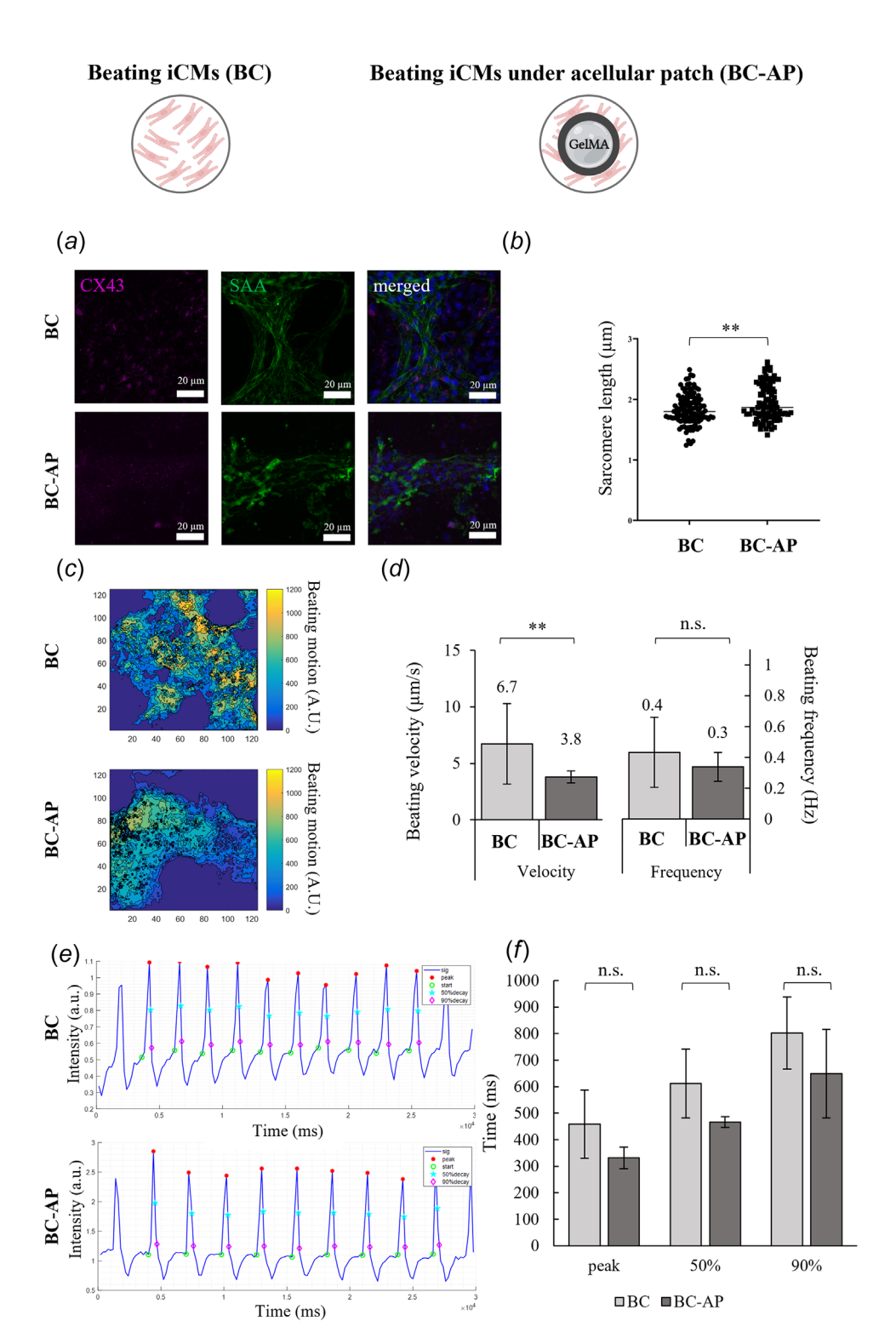


Fig. 1 Evaluation of the effect of the patch on the 2D iCM layer using cardiac protein expressions, beating characterization, and Ca^{2+} handling properties. Immunostaining characterization of patch-free beating iCMs (BC) or beating iCMs under an acellular patch (BC-AP) on day 7 (All scale bars indicate 20 μ m). (a) The Connexin 43 (CX43) staining of BC and BC-AP, the sarcomeric alphaactinin (SAA) staining of BC and BC-AP, cell nuclei are stained with DAPI, combined CX43 and SAA staining of BC and BC-AP. (b) Sarcomere length quantification in μ m. Each point represents a sarcomere. At least 10 sarcomeres per sample are quantified, n=3. (The error bars represent standard deviation, ** represents p < 0.01). (c) The heat maps showing the beating velocity magnitude (A.U.) and distribution of BC, and BC-AP. (d) Average beating velocity and frequency of BC and BC-AP. (The error bars represent standard deviation, ** represents p < 0.01, and n.s.: not significant). (e) Ca^{2+} transient profile extracted from time-lapse recordings of BC, and BC-AP. (f) Calculated time to peak intensity, 50% decay time from peak, and 90% decay time from peak of BC, and BC-AP (The error bars represent 95% confidence levels).

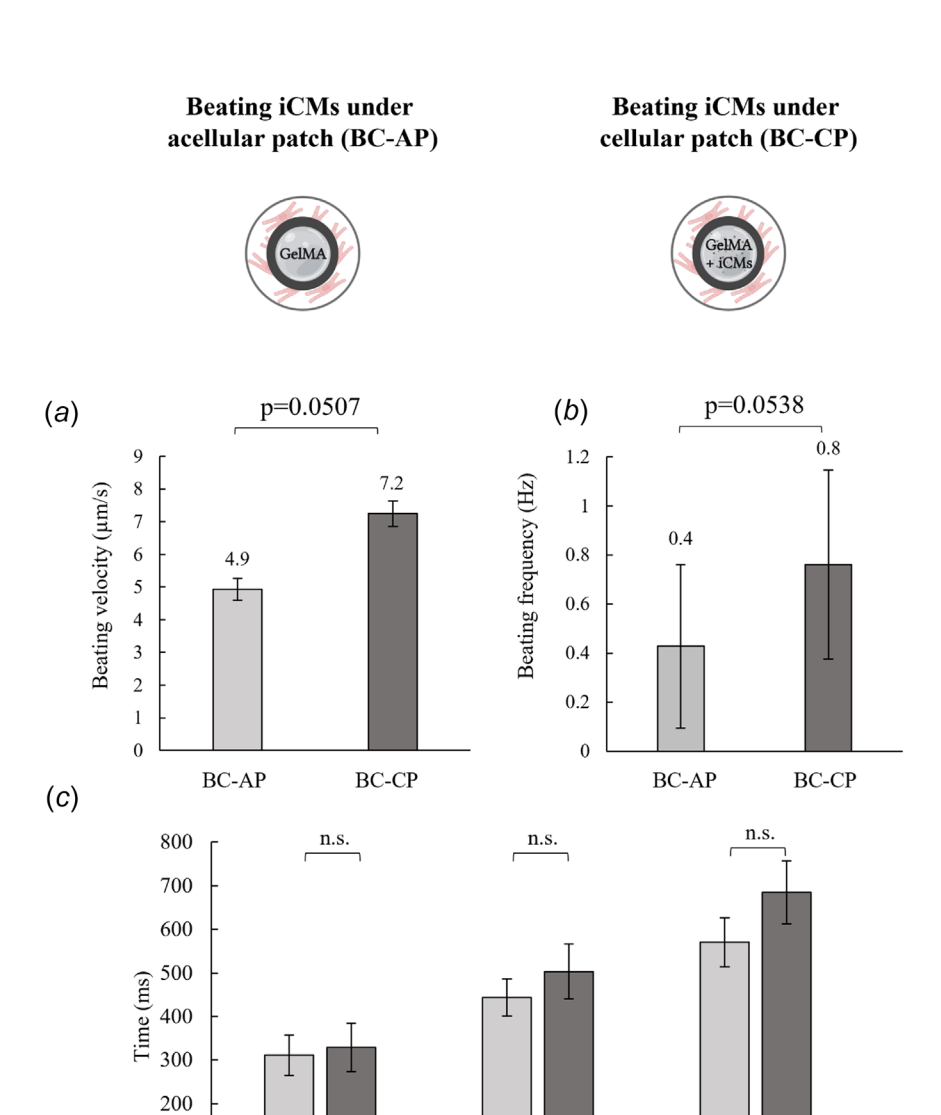


Fig. 2 Evaluation of the effect of the iCMs encapsulated in the patch on the 2D beating iCM layer on day 7. (a) Beating velocity of beating iCMs under the acellular patch (BC-AP) and the cellular patch (BC-CP). (The error bars represent standard deviation) (b) Beating frequency of BC-AP and BC-CP (The error bars represent standard deviation). Calculated time to peak intensity, 50% decay time from peak, and 90% decay time from peak of (c) BC-AP, and BC-CP (The error bars represent 95% confidence levels) (n=3).

■BC-AP ■BC-CP

50%

the bottom surface and $94.6 \, \mu m$ on the top surface of the patch (Fig. 3(a)). The maximum total displacement measured at the bottom surface corresponds to an approximately 12% strain. Using Video S1 of the Supplemental Materials on the ASME Digital Collection, the difference between the contracted and the relaxed gel was measured, and the strain was calculated as 12.5%, validating the numerical model. Similarly, the volumetric strain on the gel was zero during the relaxation state of the beating 2D iCM layer, and during contraction, it increased up to a maximum value of 0.21% (Fig. 3(b)). At the contraction state, while the gel was contracted by 0.21%, at the bottom surface, it was expanded by 0.03% at the top. Finally, the von Misses stress was calculated as zero at the relaxation state of the beating 2D iCM layer, and as 0.55 N/m² on the bottom surface and 9.36×10^{-4} N/m² on the top surface of the gel, respectively during contraction (Fig. 3(c)). As the numerical model confirms, this repetitive contraction force applied on the patch

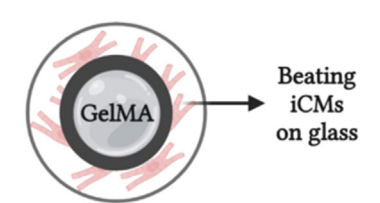
100

peak

creates a dynamic culture and hence may affect the beating characteristics of the encapsulated iCMs, which is further investigated in the following sections.

90%

Effect of Dynamic Culture on the Performance of the iCMs Encapsulated in the Patch Short-Term Gene Expression. Cellular patches in static culture (CP-SC) and dynamic culture (CP-DC) were prepared by placing them on nonbeating and beating cells, respectively, and spontaneous beating of the encapsulated cells was observed as early as the following day of encapsulation. The effect of dynamic culture created by the cyclic contraction-relaxation motion of the beating 2D iCM layer on the encapsulated iCMs' short-term cardiac-related gene expression was investigated by performing Nano-String mRNA profiling and qRT-PCR on day 7 (Fig. S2 of the Supplemental Materials). From the Nano-String data, the genes that were notably different from each other for CP-SC and



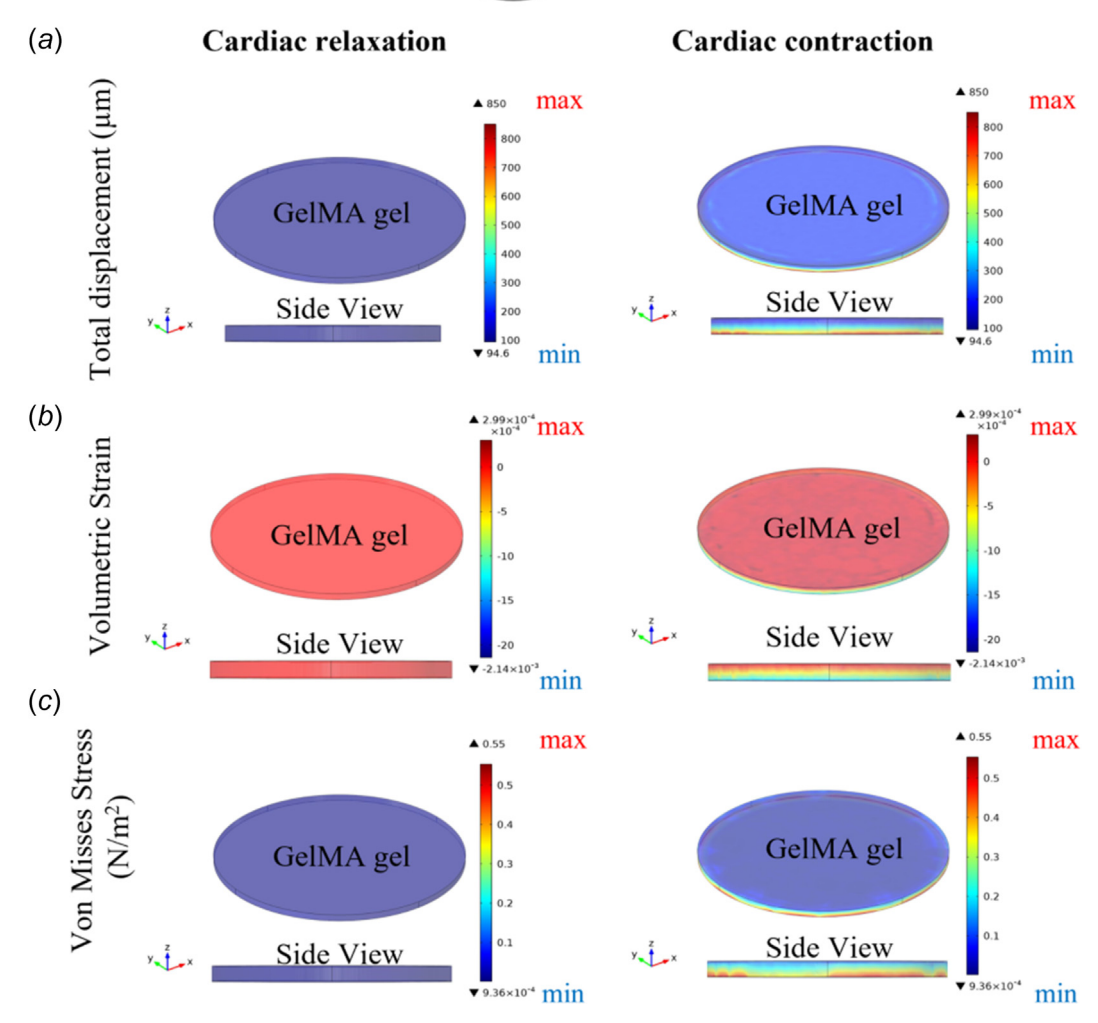


Fig. 3 Numerical analysis results for the GeIMA gel placed on the beating iCMs relaxation (left) and contraction (right): (a) The total displacement, (b) volumetric strain, and (c) von Misses stress

CP-DC are presented (Fig. S3A of the Supplemental Materials). qRT-PCR revealed no significant changes in MYH7, TNNT2, GJA1, RYR2 expressions with dynamic culture (Fig. S3B of the Supplemental Materials on the ASME Digital Collection).

Short- and Long-Term Protein Expression. To observe the effect of dynamic culture on cardiac-related protein expressions, immunostaining was performed on days 7 (short-term) and 21 (long-term). The encapsulated iCMs under both static (CP-SC) and dynamic (CP-DC) conditions showed CX43 expression and striated SAA structures for day 7 as well as day 21; however, the expression levels were more pronounced with the latter time point (Figs. 4(a) and 4(b)). CX43 was expressed in limited quantities on Day 7, but by day 21, it was expressed around the nuclei and between the cells (Fig. 4(b)). Nonetheless, no difference between CX43 expression levels of the CP-SC and CP-DC groups was observed. Average sarcomere lengths were calculated as $1.7 \pm 0.2 \,\mu\text{m}$ and $1.6 \pm 0.3 \,\mu\text{m}$ on day 7 for CP-SC and CP-DC, respectively, and $1.6 \pm 0.2 \,\mu\text{m}$ on day 21 for both CP-SC and CP-DC (Figs. 4(c) and 4(d)), indicating that average sarcomere lengths remained unaffected upon the

dynamic culture of the patch during short and long-term culture periods.

Beating Characteristics. The spontaneous beating was observed as early as 24 h after encapsulation for both CP-SC and CP-DC. To observe the effect of the beating of the underlying 2D iCM layer on the beating characteristics of the iCMs that were encapsulated in the GelMA hydrogels, BF videos were recorded on day 7 (Video S2 of the Supplemental Materials for CP-SC and Video S3 of the Supplemental Materials for CP-DC) and day 21 (Video S4 of the Supplemental Materials on the ASME Digital Collection for CP-SC and Video S5 of the Supplemental Materials for CP-DC). Analysis of the videos revealed an improvement in beating characteristics over time and with dynamic culture (Figs. 5(a) and 5(b)). For day 7, the average beating velocity was measured as $4.7 \pm 2.2 \,\mu\text{m/s}$ for CP-SC, and $5.2 \pm 3.1 \,\mu\text{m/s}$ for CP-DC (Fig. 5(c)). The average beating frequency was calculated as $0.4 \pm 0.1 \, \text{Hz}$ for CP-SC, and $0.5 \pm 0.1 \,\mathrm{Hz}$ for CP-DC. Although the beating velocity and frequency showed an increasing trend with the dynamic culture, the difference was not significant. For day 21, the average beating

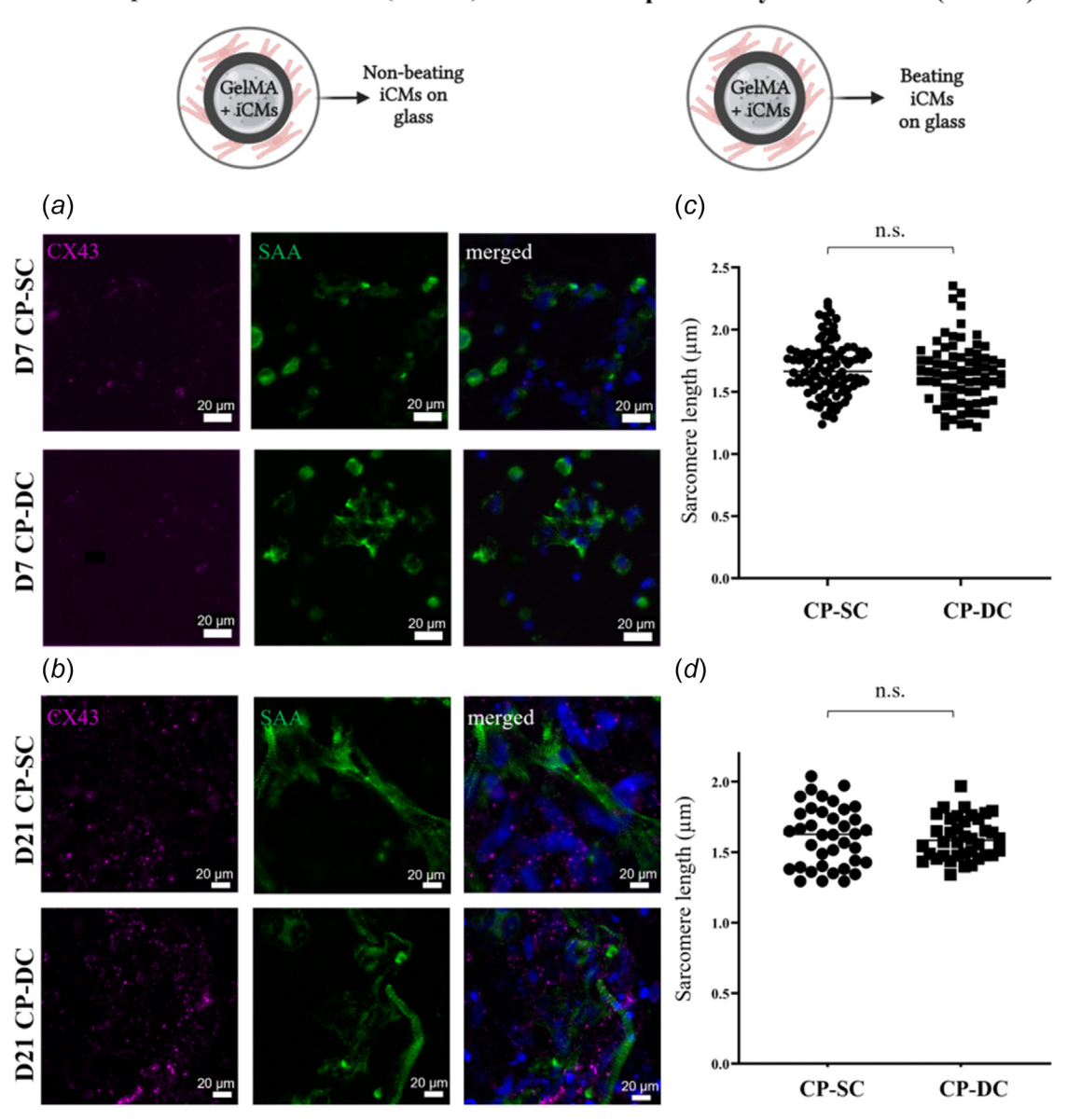


Fig. 4 Immunostaining characterization of a cellular patch in static culture (CP-SC) or dynamic culture (CP-DC) on day 7 or day 21 (All scale bars indicate 20 μ m). The Connexin 43 (CX43), the sarcomeric alpha-actinin (SAA), and combined CX43 and SAA staining of CP-SC and CP-DC (a) on day 7 and (b) on day 21. Cell nuclei are stained with DAPI. Sarcomere length quantification in μ m for (c) day 7 and (d) day 21. (n.s.: not significant) (Student's t-test) ($n \ge 3$).

velocity was quantified as $5.7 \,\mu\text{m/s} \pm 2.0 \,\mu\text{m/s}$ for CP-SC, and $6.5 \,\mu\text{m/s} \pm 3.8 \,\mu\text{m/s}$ for CP-DC (Fig. 5(d)). The average beating frequency was calculated as $0.4 \,\text{Hz} \pm 0.1 \,\text{Hz}$ for CP-SC, and $0.6 \,\text{Hz} \pm 0.1 \,\text{Hz}$ for CP-DC. Similar to day 7 results, the beating velocity improved with dynamic culture on day 21, but the change was not significant. Beating frequency, on the other hand, improved significantly with the dynamic culture (p=0.001).

 Ca^{+2} Propagation and Synchronization. The real-time Ca²⁺ transient properties of the encapsulated iCMs in static or dynamic culture were recorded as they spontaneously beat on day 7 (Videos S6 and S7 of the Supplemental Materials on the ASME Digital Collection) and day 21 (Videos S8 and S9 of the Supplemental Materials). Using the change in calcium flux intensity during the beating, the Ca²⁺ transient profiles were plotted (Figs. 6(a)–6(d)). These profiles were then utilized to calculate the time to peak flux,

50% decay time, and 90% decay time. On day 7, time to peak flux was quantified as 451.7 ± 58.0 ms for CP-SC and 521.9 ± 188.6 ms for CP-DC; 50% decay time was 692.1 ± 88.2 ms for CP-SC and 763.2 ± 182.3 ms for CP-DC, and 90% decay time was calculated to be 871.3 ± 132.4 ms for CP-SC and 953.6 ± 184.7 ms for CP-DC (Fig. 6(e)). Similarly on day 21 time to peak flux was 299.1 ± 69.9 ms for CP-SC and 290.5 ± 81.6 ms for CP-DC; 50% decay time was 432.4 ± 78.8 ms for CP-SC and 432.1 ± 70.5 ms for CP-DC; and 90% decay time was 872.0 ± 246.2 ms for CP-SC, and 611.4 ± 150.0 ms for CP-DC, respectively (Fig. 6(f)).

For a successful application, cardiac patches should be integrated with the healthy tissue such that the encapsulated cells in the patch are synchronized with the underlying beating cells comprising the healthy myocardium. The synchronization of the iCMs encapsulated in the CP-DC was assessed by analyzing the Ca²⁺ transient characteristics of the encapsulated cells and the underlying 2D

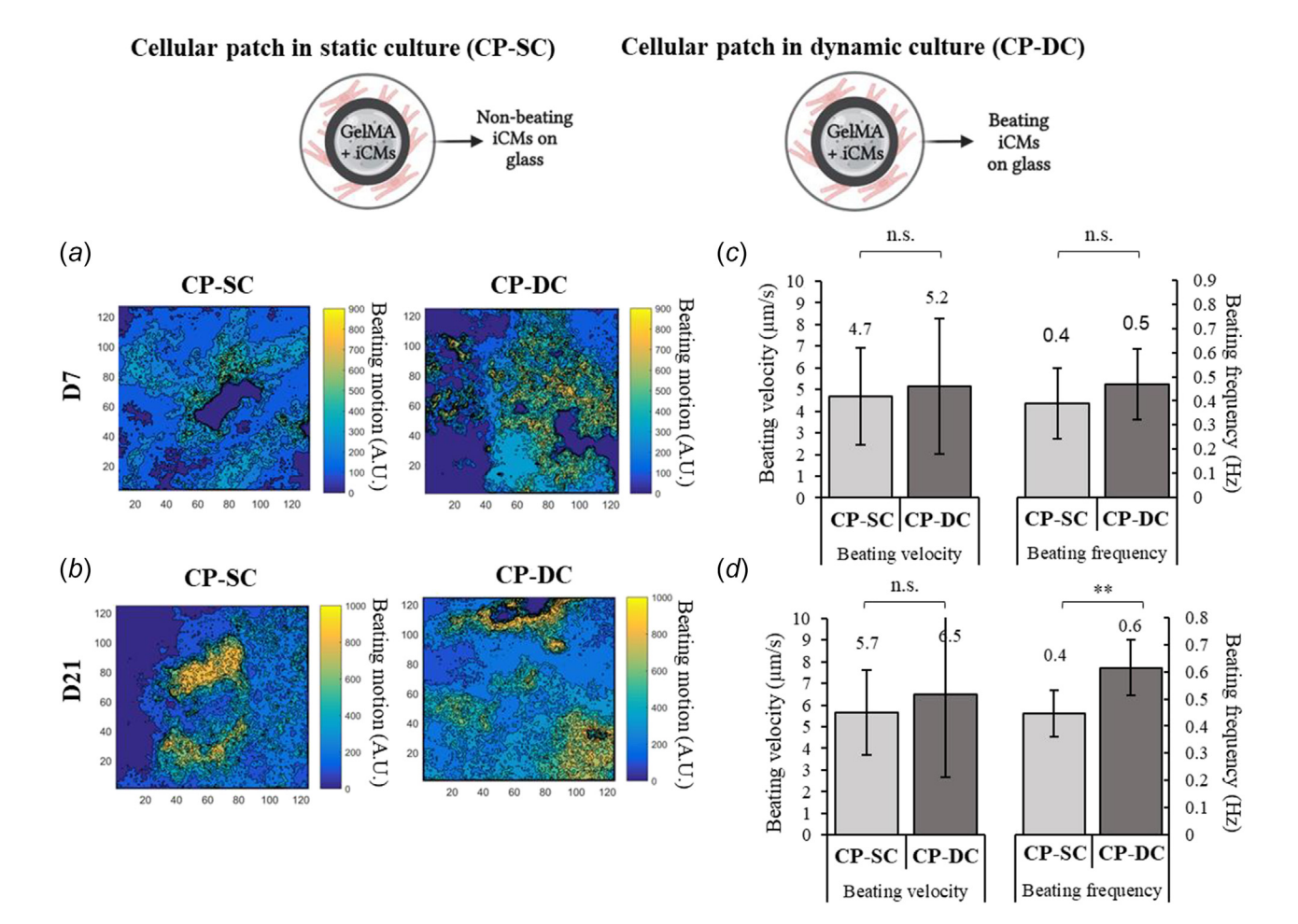


Fig. 5 The heat maps showing the beating velocity magnitude (A.U.) and distribution of encapsulated iCMs. Beating characteristics of encapsulated iCMs in static culture (CP-SC) and dynamic culture (CP-DC) (a) on day 7 and (b) on day 21. Average beating velocity and frequency of encapsulated iCMs in CP-SC and CP-DC (c) on day 7 and (d) on day 21. (** represents p < 0.01; n.s.: not significant) (Student's t-test) ($n \ge 3$). (The error bars represent standard deviation).

beating cells simultaneously. On day 7 of culture, as the cells beat spontaneously, the beating of the 2D iCM layer and iCMs encapsulated in the cellular patches were monitored in real-time for the Ca^{2+} transient propagation. At peak flux, maximum fluorescence intensity was observed (Fig. 7(a)). To evaluate the synchronicity and the Ca^{2+} propagation, the imaged area was divided into sixteen subregions. For each group, the Ca^{2+} transient profile was plotted separately, and the frequency was observed to be the same for each region (Figs. 7(b) and 7(c)). The polar histogram of Fig. 7(c) was plotted showing the spontaneous beating of each group as a periodic function, and the phase difference between each group was calculated to be less than 30° (Fig. 7(d)).

Discussion

Engineered cardiac patches have shown to be a promising regenerative treatment for the infarct region after MI. Some studies have shown that cardiac patches heal the scar tissue by evaluating the scar tissue size, angiogenesis, and beating properties after placing the patch on the scar tissue in vivo [22,25,53,54]. This study contributes to the field by providing a thorough in vitro investigation of the effect of the acellular and cellular patch on the beating properties of the underlying iCM layer, as well as the dynamic culture conditions resulting from the contraction kinetics of this iCM layer on the encapsulated iCMs in the cellular patch. Our experiments revealed a significant decrease in the beating velocity of the iCMs when an acellular patch was placed on top of them, yet the beating frequency was not affected significantly (Fig. 1(d)). Moreover, the sarcomere length of the iCMs increased when the

patch was placed on the top (Fig. 1(b)). Additionally, the time to peak, 50% decay and 90% decay decreased when the acellular patch was placed (Figs. 1(e) and 1(f)). On the other hand, when the iCMs were encapsulated in the patch (cellular patch), the beating velocity. and the frequency as well as the Ca⁺² handling properties of the underlying iCMs were increased similar to the BC level. (Fig. 2). The beating frequency of the iCMs is lower compared to human CMs, which have a beating frequency between 0.5 and 2 Hz [55]. This is expected due to the inherent immaturity of the iCMs [56]. While conducting these experiments, we observed that as the 2D iCM layer was going through the cardiac cycle, it caused a visible cyclic deformation on the patch placed on top of it. To better understand the effect of this deformation, we created a finite element model and confirmed that it closely represents the experimental measurement. (Fig. 3). We hypothesized that the dynamic culture conditions created by the cyclic deformation caused on the patch as the underlying iCM layer beats might influence the encapsulated cells in the patch. In this regard, we performed experiments to evaluate gene expression, protein expression, beating, and Ca⁺⁺ handling properties. The beating velocity and frequency of the encapsulated iCMs improved when they were kept in the dynamic culture compared to static culture (Fig. 5), yet no significant differences for the CX43 and SAA protein expression were observed (Fig. 4). Then, the effect of the dynamic culture conditions on Ca⁺ transient properties of the encapsulated iCMs on day 7 and day 21 was evaluated; however, the results were not significantly different (Fig. 6). Finally, when the Ca⁺² propagation and synchronization analysis were performed, it was observed that the encapsulated iCMs were synchronized with the underlying beating iCMs (Fig. 7).

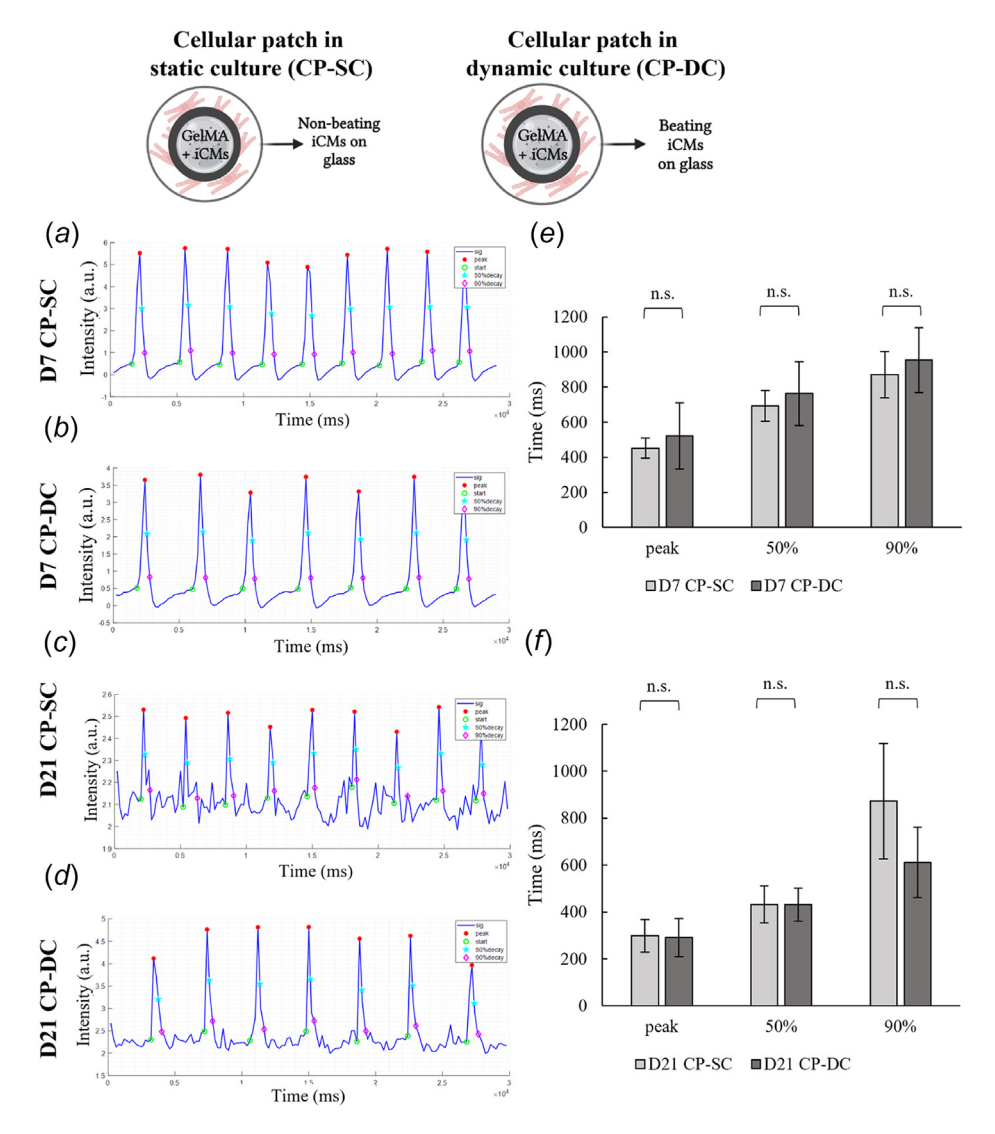


Fig. 6 Characterization of the spontaneous Ca^{2+} transient properties of iCMs when encapsulated in CP-SC or CP-DC on day 7 and day 21. Beating profile extracted from time-lapse recordings of (a) cellular patch in static culture (CP-SC) on day 7, (b) cellular patch in dynamic culture (CP-DC) on day 7, (c) CP-SC on day 21, (d) CP-DC on day 21. Calculated time to peak intensity, 50% decay time from peak, and 90% decay time from peak of (e) CP-SC and CP-DC on day 7, (f) CP-SC and CP-DC on day 21. The error bars represent 95% confidence levels. (n=3).

Cardiac patches have previously been shown to have a therapeutic effect on the infarct region [16,57,58], however here we showed that after placing an acellular patch on the beating 2D iCM layer, the beating velocity, as well as the frequency, decreased. This is most probably due to the patch's weight, disturbance during placement, and prevention of the underlying iCMs from accessing oxygen and nutrients (Fig. 1(d)). Additionally, the average sarcomere length of the underlying iCMs increased significantly (Fig. 1(b)) with a value of $1.98 \pm 0.3 \,\mu m$ and it is the closest to human adult sarcomere length [59]. Although it has not been shown in the literature before, this increase might be a result of the load induced due to the weight of the patch, and the beating tissue is required to overcome this load as it contracts. Yet, these effects can be minimized by creating a gridlike patch shape, which is one of the most commonly used patch shapes [28,60,61]. We also hypothesized that including iCMs in the patch will help the underlying iCM layer to regain their former beating characteristics and was able to show that inclusion of the cells in the patch helped minimize the adverse effects we observed with the acellular patch and improved the beating characteristics and Ca⁺² transient properties to a level of 2D iCM layer without the patch (Fig. 2). This observation is in parallel with the findings from the literature [10,62] and is most likely resulting from the released secretion of the encapsulated iCMs [57,63,64] (Fig. 2). Although the difference was not statistically significant the p value was very close to 0.05, indicating that placing the iCMs in the patch improves the beating velocity and frequency and the results will be significant with improving the sample size.

To better understand and observe the deformation of the patch caused by the contraction kinetics of the underlying beating iCM layer, a simple finite element model was created. The contraction force was measured experimentally and used as an input for the applied load by the cells on the patch and as a result, a model that closely represents the authentic conditions was generated. From the numerical analysis, it was apparent that the total displacement (Fig. 3(a)) and Von Misses stress (Fig. 3(c)) was maximum on the bottom surface of the patch and minimum on the top surface of the patch. This was expected since the contraction of the cells directly affects the bottom surface of the patch. The volumetric strain result showed a negative strain on the bottom surface of the patch, which resulted from the contraction of the beating iCM layer (Fig. 3(b)). Additionally, the calculated deformation corresponded to a cyclic elongation of almost 12%, which is in a similar range of what has

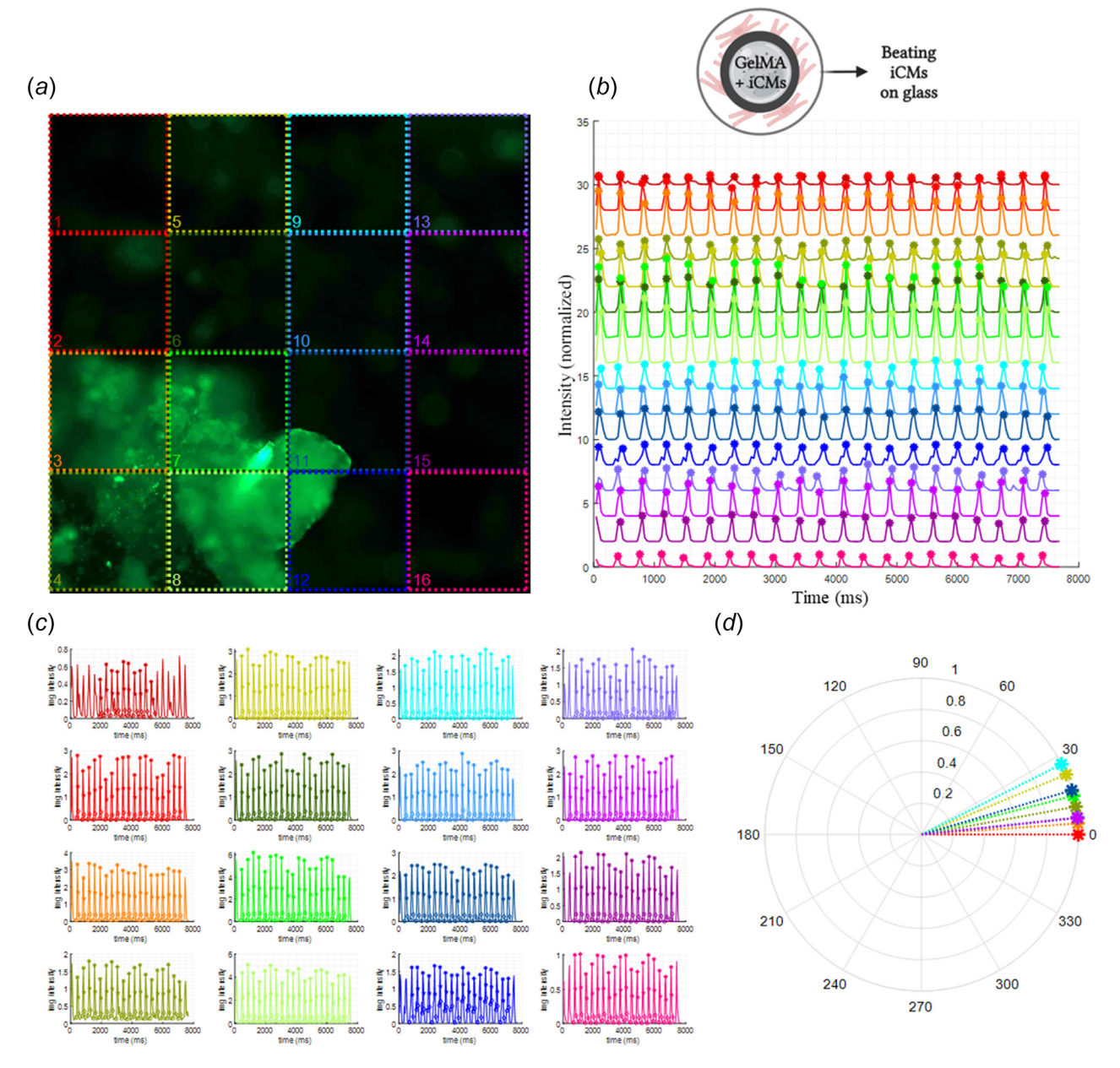


Fig. 7 Synchronization analysis on day 7. (a) A representative snapshot from calcium flux time-lapse recording (the image was divided into 16 groups and each group was represented with a different color), (b) Ca^{2+} transient profile of each designated group as extracted from these time-lapse recordings, (c) Ca^{2+} transient profile of each group separately indicating the beating frequencies, (d) Polar histogram of the phase difference shown in (c).

been previously reported for the mechanical simulation studies conducted with cardiomyocytes (8%–15%) [56,65–67].

For a comprehensive understanding, the effect of this dynamic culture condition created by the cyclic contraction and relaxation of the underlying beating iCM layer on the encapsulated iCMs in the cellular patch was further investigated. For that reason, first, transcriptome and qRT-PCR analysis were performed after exposing the cellular patch to dynamic and static culture for 7 days, and no significant change was observed.

After evaluating the effect on gene expression levels, immunostaining was performed to investigate the effect of dynamic culture on encapsulated iCMs' sarcomere structure and CX43 expression. Immunostaining results revealed that CX43 expression increased from day 7 to day 21 (Figs. 4(a) and 4(b)). Moreover, on day 21, CX43 expression was expressed at higher levels and observed to be more localized between the cells for CP-DC compared to CP-SC (Fig. 4(b)). It is well-known that CX43 is a gap-junction protein and plays a crucial part in the synchronous contraction of the CMs.

Therefore, increased expression of CX43 along with localization on the cell boundaries demonstrates a better connected iCM network [68]. Our results are in alignment with previous studies where CX43 expression was more concentrated between cells when mechanical stretch was applied (10% elongation, 3 Hz) [69] and increased with a stretch of 10% at 1 Hz [70].

Additionally, it has been previously reported through the analysis of sarcomere elongation, alignment, and Z-bands that mechanical stretching improves structural maturity along with culture time [71]. In this study, we investigated the structural organization by staining SAA and measuring the sarcomere length (Fig. 4). Although the measured values were slightly lower than the sarcomere length of human adult CMs (over 2 μ m, [59]), they were in the same range as previously reported numbers for human or mouse-derived CMs (range: 1.6–2.2 μ m) [31,72,73]. On day 7, CP-DC sarcomeres were visibly more striated, which is an indication of more developed cells. Furthermore, sarcomeres were observed to be more striated on day 21 compared to day 7 for both CP-SC and CP-DC.

Analysis of the beating characteristics demonstrated an increase (although not significant) in beating velocity of CP-DC compared to CP-SC for both day 7 and day 21 (Fig. 5). When the beating frequencies were compared, on day 21 a significant increase was observed for CP-DC (Fig. 5(d)). Previously it was reported that cyclic stretching significantly improved the beating rate of the iCMs encapsulated in collagen gels [74]. Most of the other studies stimulated iCMs using uni-axial stretching or electrical stimulation at a certain frequency and did not report the spontaneous beating properties [56,75]. In the present study, when the underlying beating cell layer contracted, it deformed the gel in every direction and the deformation decreased from the bottom surface of the gel toward the top, whereas the previous studies applied a homogenous uni-axial stretch. This discrepancy might be the reason for not seeing a significant increase in beating velocity between CP-DC and CP-SC.

Finally, the Ca²⁺ transient properties of the CP-SC and CP-DC were investigated by plotting the Ca²⁺ intensity profiles and deriving the required time to peak, 50% decay, and 90% decay. On day 7, all these values were measured to be longer for CP-DC when compared to CP-SC. Previous studies related this prolonged duration with maturity [46,72,76]. On day 21, time to peak and time to 50% decay values were almost the same, whereas time to 90% decay was shortened for CP-DC compared to CP-SC (Fig. 6).

In addition to the Ca²⁺ handling properties of the CP-DC, the Ca²⁺ propagation, as well as synchronization of the encapsulated cells with the underlying 2D iCM layer were explored. For three different samples, we observed that the cells in the gel synchronized with the beating 2D iCM layer (Fig. 7). This was an important aspect to show in vitro because arrhythmias after transplantation are one of the greatest concerns of using immature iCMs in clinical studies [77]. Additionally, even though a number of previous studies have evaluated the compatibility, conduction velocity, and Ca²⁺ transient properties of CMs seeded on cardiac patches engineered using conductive materials [29,78] or using various methods [19], the present study is the first to explore the communication and synchronization between the iCMs encapsulated in the patch and the underlying beating 2D iCM layer. Moreover, our results revealed a phase difference between the groups up to 30 deg, which can be explained by the time required to transport the electrical signal between the cells. This observation was an indication of the synchronization between the iCMs encapsulated in the patch and the underlying beating iCMs. Previous studies from our lab and other labs reported this phenomenon using cardiac fibroblasts and showed that although they can propagate electrical conduction, it is slower and thus result in phase differences [52,79-81].

This study is limited by the fact that iCMs being inherently immature compared to adult CMs, and the beating characteristics are significantly lower. Additionally, in the future, it might be beneficial to increase the healthy tissue to patch ratio. Moreover, the effect of using different materials while preparing the patch can be investigated as a future work. Finally, the underlying iCMs can be aligned in 2D, or a three-dimensional beating tissue model can be developed to create more mimetic "healthy beating tissue model".

Conclusion

Overall, in this study, we investigated the interrelation between 2D beating iCM layer and a cardiac patch. We showed that although placing an acellular patch on the beating 2D iCM layer affected the beating properties negatively, via encapsulation of iCMs in the patch the beating characteristics were recovered, which demonstrates the importance of using cells, specifically iCMs, in the cardiac patches. We developed a model to computationally verify the deformation of the gel caused by the contraction of the underlying beating cells. Considering our results, we concluded that the cyclic contraction-relaxation of the beating 2D iCM layer creates a dynamic culture, but it does not significantly improve cardiac-related gene expressions, beating velocity on day 7 and 21, and the beating frequency on day 7, of the encapsulated iCMs in the cellular patch. This study reports a comprehensive understanding of how an acellular or

cellular patch affects the beating of the 2D iCM layer and how the beating of this layer effect the iCMs encapsulated in the patch, which can inform approaches to engineer therapeutic cardiac patches.

Acknowledgment

Figures were created using Bio-Render.

Funding Data

- National Institute of Health (NIH) (Award No. R01 HL141909-01A1; Funder ID: 10.13039/100000002).
- National Science Foundation (NSF) (Award No. 1651385; Funder ID: 10.13039/100000001).

References

- Heron, M., 2019, "Deaths: Leading Causes for 2017," Natl. Vital Stat. Rep., 68(6), pp. 1–77.
- [2] Thomas, H., Diamond, J., Vieco, A., Chaudhuri, S., Shinnar, E., Cromer, S., Perel, P., et al., 2018, "Global Atlas of Cardiovascular Disease 2000-2016: The Path to Prevention and Control," Global Heart, 13(3), p. 143.
- [3] Gorenek, B., Blomström Lundqvist, C., Brugada Terradellas, J., Camm, A. J., Hindricks, G., Huber, K., Kirchhof, P., et al., 2014, "Cardiac Arrhythmias in Acute Coronary Syndromes: Position Paper From the Joint EHRA, ACCA, and EAPCI Task Force," EP Europace, 16(11), pp. 1655–1673.
- [4] Henkel, D. M., Witt, B. J., Gersh, B. J., Jacobsen, S. J., Weston, S. A., Meverden, R. A., and Roger, V. L., 2006, "Ventricular Arrhythmias After Acute Myocardial Infarction: A 20-Year Community Study," Am. Heart J., 151(4), pp. 806–812.
- Infarction: A 20-Year Community Study," Am. Heart J., 151(4), pp. 806–812.
 [5] Lalit, P. A., Hei, D. J., Raval, A. N., and Kamp, T. J., 2014, "Induced Pluripotent Stem Cells for Post–Myocardial Infarction Repair," Circ. Res., 114(8), pp. 1328–1345.
- [6] Oh, H., Bradfute, S. B., Gallardo, T. D., Nakamura, T., Gaussin, V., Mishina, Y., Pocius, J., Michael, L. H., et al., 2003, "Cardiac Progenitor Cells From Adult Myocardium: Homing, Differentiation, and Fusion After Infarction," Proc. Natl. Acad. Sci. USA, 100(21), pp. 12313–12318.
- [7] Guo, Y., Yu, Y., Hu, S., Chen, Y., and Shen, Z., 2020, "The Therapeutic Potential of Mesenchymal Stem Cells for Cardiovascular Diseases," Cell Death Dis., 11(5), pp. 1–10.
- [8] Traverse, J. H., Henry, T. D., Dib, N., Patel, A. N., Pepine, C., Schaer, G. L., DeQuach, J. A., et al., 2019, "First-in-Man Study of a Cardiac Extracellular Matrix Hydrogel in Early and Late Myocardial Infarction Patients," JACC: Basic Transl. Sci., 4(6), pp. 659–669.
- [9] Chen, M. H., Chung, J. J., Mealy, J. E., Zaman, S., Li, E. C., Arisi, M. F., Atluri, P., and Burdick, J. A., 2019, "Injectable Supramolecular Hydrogel/Microgel Composites for Therapeutic Delivery," Macromol. Biosci., 19(1), p. e1800248.
- [10] Mei, X., and Cheng, K., 2020, "Recent Development in Therapeutic Cardiac Patches," Front. Cardiovasc. Med., 7, p. 610364.
- [11] Basara, G., Bahcecioglu, G., Ozcebe, S. G., Ellis, B. W., Ronan, G., and Zorlutuna, P., 2022, "Myocardial Infarction From a Tissue Engineering and Regenerative Medicine Point of View: A Comprehensive Review on Models and Treatments," Biophys. Rev., 3(3), p. 031305.
- [12] Yoshizumi, T., Zhu, Y., Jiang, H., D'Amore, A., Sakaguchi, H., Tchao, J., Tobita, K., and Wagner, W. R., 2016, "Timing Effect of Intramyocardial Hydrogel Injection for Positively Impacting Left Ventricular Remodeling After Myocardial Infarction," Biomaterials, 83, pp. 182–193.
- [13] Yu, D., Wang, X., and Ye, L., 2021, "Cardiac Tissue Engineering for the Treatment of Myocardial Infarction," J. Cardiovasc. Develop. Disease, 8(11), p. 153.
- [14] Zimmermann, W.-H., 2020, "Tissue Engineered Heart Repair From Preclinical Models to First-in-Patient Studies," Curr. Opin. Physiol., 14, pp. 70–77.
- [15] Tiburcy, M., Hudson, J. E., Balfanz, P., Schlick, S., Meyer, T., Liao, M.-L. C., Levent, E., et al., 2017, "Defined Engineered Human Myocardium With Advanced Maturation for Applications in Heart Failure Modelling and Repair," Circulation, 135(19), pp. 1832–1847.
- [16] Das, S., Nam, H., and Jang, J., 2021, "3D Bioprinting of Stem Cell-Laden Cardiac Patch: A Promising Alternative for Myocardial Repair," APL Bioeng., 5(3), p. 031508.
- [17] Serpooshan, V., Zhao, M., Metzler, S. A., Wei, K., Shah, P. B., Wang, A., Mahmoudi, M., et al., 2013, "The Effect of Bioengineered Acellular Collagen Patch on Cardiac Remodeling and Ventricular Function Post Myocardial Infarction," Biomaterials, 34(36), pp. 9048–9055.
- [18] Scully, B. B., Fan, C., Grigoryan, B., Jacot, J. G., Vick, G. W., Kim, J. J., Fraser, C. D., et al., 2016, "Remodeling of ECM Patch Into Functional Myocardium in an Ovine Model: A Pilot Study," J. Biomed. Mater. Res. Part B: Appl. Biomater., 104(8), pp. 1713–1720.
- [19] Sharma, D., Ferguson, M., Kamp, T. J., and Zhao, F., 2019, "Constructing Biomimetic Cardiac Tissues: A Review of Scaffold Materials for Engineering Cardiac Patches," Emergent Mater., 2(2), pp. 181–191.
- [20] Song, X., Wang, X., Zhang, J., Shen, S., Yin, W., Ye, G., Wang, L., Hou, H., and Qiu, X., 2021, "A Tunable Self-Healing Ionic Hydrogel With Microscopic Homogeneous Conductivity as a Cardiac Patch for Myocardial Infarction Repair," Biomaterials, 273, p. 120811.
- [21] Jiang, Y., Sun, S.-J., Zhen, Z., Wei, R., Zhang, N., Liao, S.-Y., and Tse, H.-F., 2021, "Myocardial Repair of Bioengineered Cardiac Patches With Decellularized Placental Scaffold and Human-Induced Pluripotent Stem Cells in a Rat Model of Myocardial Infarction," Stem Cell Res. Ther., 12(1), p. 13.

- [22] Gao, L., Kupfer, M. E., Jung, J. P., Yang, L., Zhang, P., Tran, Q., Ajeti, V., et al., 2017, "Myocardial Tissue Engineering With Cells Derived From Human-Induced Pluripotent Stem Cells and a Native-Like, High-Resolution, 3-Dimensionally Printed Scaffold," Circ. Res., 120(8), 1318–1325.
- [23] de Abreu, R. C., Fernandes, H., da Costa Martins, P. A., Sahoo, S., Emanueli, C., and Ferreira, L., 2020, "Native and Bioengineered Extracellular Vesicles for Cardiovascular Therapeutics," Nat. Rev. Cardiol., 17(11), pp. 685–697.
- [24] Firoozi, S., Pahlavan, S., Ghanian, M.-H., Rabbani, S., Barekat, M., Nazari, A., Pakzad, M., et al., 2020, "Mesenchymal Stem Cell-Derived Extracellular Vesicles Alone or in Conjunction With a SDKP-Conjugated Self-Assembling Peptide Improve a Rat Model of Myocardial Infarction," Biochem. Biophys. Res. Commun., 524(4), pp. 903–909.
- [25] Liu, X., De la Cruz, E., Gu, X., Balint, L., Oxendine-Burns, M., Terrones, T., Ma, W., et al., 2020, "Lymphoangiocrine Signals Promote Cardiac Growth and Repair," Nature, 588(7839), pp. 705–711.
- [26] McMahan, S., Taylor, A., Copeland, K. M., Pan, Z., Liao, J., and Hong, Y., 2020, "Current Advances in Biodegradable Synthetic Polymer Based Cardiac Patches," J. Biomed. Mater. Res. Part A, 108(4), pp. 972–983.
- [27] Bejleri, D., and Davis, M. E., 2019, "Decellularized Extracellular Matrix Materials for Cardiac Repair and Regeneration," Adv. Healthcare Mater., 8(5), p. 1801217.
- [28] Bejleri, D., Streeter, B. W., Nachlas, A. L. Y., Brown, M. E., Gaetani, R., Christman, K. L., and Davis, M. E., 2018, "A Bioprinted Cardiac Patch Composed of Cardiac-Specific Extracellular Matrix and Progenitor Cells for Heart Repair," Adv. Healthcare Mater., 7(23), p. 1800672.
- [29] Walker, B. W., Lara, R. P., Yu, C. H., Sani, E. S., Kimball, W., Joyce, S., and Annabi, N., 2019, "Engineering a Naturally-Derived Adhesive and Conductive Cardiopatch," Biomaterials, 207, pp. 89–101.
- [30] Guo, B., and Ma, P. X., 2018, "Conducting Polymers for Tissue Engineering," Biomacromolecules, 19(6), pp. 1764–1782.
- [31] Basara, G., Saeidi-Javash, M., Ren, X., Bahcecioglu, G., Wyatt, B. C., Anasori, B., Zhang, Y., and Zorlutuna, P., 2020, "Electrically Conductive 3D Printed Ti3C2Tx MXene-PEG Composite Constructs for Cardiac Tissue Engineering," Acta Biomater., 139, pp. 179–189.
- [32] Shin, S. R., Jung, S. M., Zalabany, M., Kim, K., Zorlutuna, P., Bok Kim, S., Nikkhah, M., et al., 2013, "Carbon-Nanotube-Embedded Hydrogel Sheets for Engineering Cardiac Constructs and Bioactuators," ACS Nano, 7(3), pp. 2369–2380.
- [33] Hitscherich, P., Aphale, A., Gordan, R., Whitaker, R., Singh, P., Xie, L., Patra, P., and Lee, E. J., 2018, "Electroactive Graphene Composite Scaffolds for Cardiac Tissue Engineering: Electroactive Graphene Composite Scaffolds for Cardiac Tissue Engineering," J. Biomed. Mater. Res. Part A, 106(11), pp. 2923–2933.
- [34] Malki, M., Fleischer, S., Shapira, A., and Dvir, T., 2018, "Gold Nanorod-Based Engineered Cardiac Patch for Suture-Free Engraftment by Near IR," Nano Lett., 18(7), pp. 4069–4073.
- [35] Chen, H., Fan, L., Peng, N., Yin, Y., Mu, D., Wang, J., Meng, R., and Xie, J., 2022, "Galunisertib-Loaded Gelatin Methacryloyl Hydrogel Microneedle Patch for Cardiac Repair After Myocardial Infarction," ACS Appl. Mater Interfaces, 14(36), pp. 40491–40500.
- [36] Basara, G., Ozcebe, S. G., Ellis, B. W., and Zorlutuna, P., 2021, "Tunable Human Myocardium Derived Decellularized Extracellular Matrix for 3D Bioprinting and Cardiac Tissue Engineering," Gels, 7(2), p. 70.
- [37] Nichol, J. W., Koshy, S. T., Bae, H., Hwang, C. M., Yamanlar, S., and Khademhosseini, A., 2010, "Cell-Laden Microengineered Gelatin Methacrylate Hydrogels," Biomaterials, 31(21), pp. 5536–5544.
- [38] Jackman, C. P., Ganapathi, A. M., Asfour, H., Qian, Y., Allen, B. W., Li, Y., and Bursac, N., 2018, "Engineered Cardiac Tissue Patch Maintains Structural and Electrical Properties After Epicardial Implantation," Biomaterials, 159, pp. 48, 58
- [39] Noguchi, R., Nakayama, K., Itoh, M., Kamohara, K., Furukawa, K., Oyama, J., Node, K., and Morita, S., 2016, "Development of a Three-Dimensional Pre-Vascularized Scaffold-Free Contractile Cardiac Patch for Treating Heart Disease," J. Heart Lung Transplant., 35(1), pp. 137–145.
- [40] Gao, L., Gregorich, Z. R., Zhu, W., Mattapally, S., Oduk, Y., Lou, X., Kannappan, R., et al., 2018, "Large Cardiac-Muscle Patches Engineered From Human Induced-Pluripotent Stem-Cell-Derived Cardiac Cells Improve Recovery From Myocardial Infarction in Swine," Circulation, 137(16), pp. 1712–1730.
 [41] Yeung, E., Fukunishi, T., Bai, Y., Bedja, D., Pitaktong, I., Mattson, G., Jeyaram,
- [41] Yeung, E., Fukunishi, T., Bai, Y., Bedja, D., Pitaktong, I., Mattson, G., Jeyaram, A., et al., 2019, "Cardiac Regeneration Using Human-Induced Pluripotent Stem Cell-Derived Biomaterial-Free 3D-Bioprinted Cardiac Patch In Vivo," J. Tissue Eng. Regener. Med., 13(11), pp. 2031–2039.
- [42] Tang, J., Wang, J., Huang, K., Ye, Y., Su, T., Qiao, L., Hensley, M. T., et al., 2018, "Cardiac Cell–Integrated Microneedle Patch for Treating Myocardial Infarction," Sci. Adv., 4(11), p. eaat9365.
- [43] Kadota, S., Pabon, L., Reinecke, H., and Murry, C. E., 2017, "In Vivo Maturation of Human Induced Pluripotent Stem Cell-Derived Cardiomyocytes in Neonatal and Adult Rat Hearts," Stem Cell Rep., 8(2), pp. 278–289.
- [44] Cho, G.-S., Lee, D. I., Tampakakis, E., Murphy, S., Andersen, P., Uosaki, H., Chelko, S., et al., 2017, "Neonatal Transplantation Confers Maturation of PSC-Derived Cardiomyocytes Conducive to Modeling Cardiomyopathy," Cell Rep., 18(2), pp. 571–582.
- [45] Lian, X., Zhang, J., Azarin, S. M., Zhu, K., Hazeltine, L. B., Bao, X., Hsiao, C., Kamp, T. J., and Palecek, S. P., 2013, "Directed Cardiomyocyte Differentiation From Human Pluripotent Stem Cells by Modulating Wnt/β-Catenin Signaling Under Fully Defined Conditions," Nat. Protoc., 8(1), pp. 162–175.
- [46] Acun, A., Nguyen, T. D., and Zorlutuna, P., 2019, "In Vitro Aged, hiPSC-Origin Engineered Heart Tissue Models With Age-Dependent Functional Deterioration to Study Myocardial Infarction," Acta Biomater., 94, pp. 372–391.

- [47] Ellis, B. W., Acun, A., Can, U. I., and Zorlutuna, P., 2017, "Human iPSC-Derived Myocardium-on-Chip With Capillary-Like Flow for Personalized Medicine," Biomicrofluidics, 11(2), p. 024105.
- [48] Yue, X., Nguyen, T. D., Zellmer, V., Zhang, S., and Zorlutuna, P., 2018, "Stromal Cell-Laden 3D Hydrogel Microwell Arrays as Tumor Microenvironment Model for Studying Stiffness Dependent Stromal Cell-Cancer Interactions," Biomaterials, 170, pp. 37–48.
- [49] Lee, D., Zhang, H., and Ryu, S., 2019, "Elastic Modulus Measurement of Hydrogels," *Cellulose-Based Superabsorbent Hydrogels*, Md. I. H. Mondal ed., Springer International Publishing, Cham, pp. 865–884.
- [50] Nagarajan, N., Vyas, V., Huey, B. D., and Zorlutuna, P., 2016, "Modulation of the Contractility of Micropatterned Myocardial Cells With Nanoscale Forces Using Atomic Force Microscopy," Nanobiomedicine, 3, p. 184954351667534.
- [51] Nguyen, D. T., Nagarajan, N., and Zorlutuna, P., 2018, "Effect of Substrate Stiffness on Mechanical Coupling and Force Propagation at the Infarct Boundary," Biophys. J., 115(10), pp. 1966–1980.
- [52] Ji, J., Ren, X., and Zorlutuna, P., 2021, "Cardiac Cell Patterning on Customized Microelectrode Arrays for Electrophysiological Recordings," Micromachines, 12(11), p. 1351.
- [53] Yang, Y., Lei, D., Huang, S., Yang, Q., Song, B., Guo, Y., Shen, A., Yuan, Z., Li, S., Qing, F.-L., Ye, X., You, Z., and Zhao, Q., 2019, "Elastic 3D-Printed Hybrid Polymeric Scaffold Improves Cardiac Remodeling After Myocardial Infarction," Adv. Healthcare Mater., 8(10), p. 1900065.
- [54] He, Y., Hou, H., Wang, S., Lin, R., Wang, L., Yu, L., and Qiu, X., 2021, "From Waste of Marine Culture to Natural Patch in Cardiac Tissue Engineering," Bioactive Mater., 6(7), pp. 2000–2010.
- [55] Cohen, O., and Safran, S. A., 2018, "Theory of Frequency Response of Mechanically Driven Cardiomyocytes," Sci. Rep., 8(1), p. 2237.
- [56] LaBarge, W., Mattappally, S., Kannappan, R., Fast, V. G., Pretorius, D., Berry, J. L., and Zhang, J., 2019, "Maturation of Three-Dimensional, hiPSC-Derived Cardiomyocyte Spheroids Utilizing Cyclic, Uniaxial Stretch and Electrical Stimulation," PLoS One, 14(7), p. e0219442.
- [57] Chow, A., Stuckey, D. J., Kidher, E., Rocco, M., Jabbour, R. J., Mansfield, C. A., Darzi, A., et al., 2017, "Human Induced Pluripotent Stem Cell-Derived Cardiomyocyte Encapsulating Bioactive Hydrogels Improve Rat Heart Function Post Myocardial Infarction," Stem Cell Rep., 9(5), pp. 1415–1422.
- [58] Su, T., Huang, K., Mathews, K. G., Scharf, V. F., Hu, S., Li, Z., Frame, B. N., et al., 2020, "Cardiac Stromal Cell Patch Integrated With Engineered Microvessels Improves Recovery From Myocardial Infarction in Rats and Pigs," ACS Biomater. Sci, Eng., 6(11), pp. 6309–6320.
- [59] Dias, T. P., Pinto, S. N., Santos, J. I., Fernandes, T. G., Fernandes, F., Diogo, M. M., Prieto, M., and Cabral, J. M. S., 2018, "Biophysical Study of Human Induced Pluripotent Stem Cell-Derived Cardiomyocyte Structural Maturation During Long-Term Culture," Biochem. Biophys. Res. Commun., 499(3), pp. 611–617.
- [60] Kim, K. S., Joo, H. J., Choi, S.-C., Kim, J.-H., Park, C.-Y., Song, M.-H., Noh, J.-M., et al., 2021, "Transplantation of 3D Bio-Printed Cardiac Mesh Improves Cardiac Function and Vessel Formation Via ANGPT1/Tie2 Pathway in Rats With Acute Myocardial Infarction," Biofabrication, 13(4), p. 045014.
- [61] Streeter, B. W., and Davis, M. E., 2019, "Therapeutic Cardiac Patches for Repairing the Myocardium," *Cell Biology and Translational Medicine*, K. Turksen ed., Vol. 5, Stem Cells: Translational Science to Therapy, Springer International Publishing, Cham, pp. 1–24.
- [62] Lee, J., Stagg, M. A., Siedlecka, U., Latif, N., Soppa, G. K., Yacoub, M., and Terracciano, C. M., 2008, "Identification of Cell-Specific Soluble Mediators and Cellular Targets During Cell Therapy for the Treatment of Heart Failure," Regenerative Med., 3(6), pp. 953–962.
- [63] Citro, L., Naidu, S., Hassan, F., Kuppusamy, M. L., Kuppusamy, P., Angelos, M. G., and Khan, M., 2014, "Comparison of Human Induced Pluripotent Stem-Cell Derived Cardiomyocytes With Human Mesenchymal Stem Cells Following Acute Myocardial Infarction," PLoS One, 9(12), p. e116281.
- [64] Shiba, Y., Gomibuchi, T., Seto, T., Wada, Y., Ichimura, H., Tanaka, Y., Ogasawara, T., et al., 2016, "Allogeneic Transplantation of iPS Cell-Derived Cardiomyocytes Regenerates Primate Hearts," Nature, 538(7625), pp. 388–391.
- [65] Zhang, W., Kong, C. W., Tong, M. H., Chooi, W. H., Huang, N., Li, R. A., and Chan, B. P., 2017, "Maturation of Human Embryonic Stem Cell-Derived Cardiomyocytes (hESC-CMs) in 3D Collagen Matrix: Effects of Niche Cell Supplementation and Mechanical Stimulation," Acta Biomater., 49, pp. 204–217.
- [66] Ovchinnikova, E., Hoes, M., Ustyantsev, K., Bomer, N., de Jong, T. V., van der Mei, H., Berezikov, E., and van der Meer, P., 2018, "Modeling Human Cardiac Hypertrophy in Stem Cell-Derived Cardiomyocytes," Stem Cell Rep., 10(3), pp. 794–807.
- [67] Kreutzer, J., Viehrig, M., Pölönen, R.-P., Zhao, F., Ojala, M., Aalto-Setälä, K., and Kallio, P., 2020, "Pneumatic Unidirectional Cell Stretching Device for Mechanobiological Studies of Cardiomyocytes," Biomech. Model Mechanobiol., 19(1), pp. 291–303.
- [68] Michela, P., Velia, V., Aldo, P., and Ada, P., 2015, "Role of Connexin 43 in Cardiovascular Diseases," Eur. J. Pharmacol., 768, pp. 71–76.
- [69] Shimko, V. F., and Claycomb, W. C., 2008, "Effect of Mechanical Loading on Three-Dimensional Cultures of Embryonic Stem Cell-Derived Cardiomyocytes," Tissue Eng Part A, 14(1), pp. 49–58.
- [70] Kensah, G., Roa Lara, A., Dahlmann, J., Zweigerdt, R., Schwanke, K., Hegermann, J., Skvorc, D., et al., 2013, "Murine and Human Pluripotent Stem Cell-Derived Cardiac Bodies Form Contractile Myocardial Tissue In Vitro," Eur. Heart J., 34(15), pp. 1134–1146.
- [71] Gu, X., Zhou, F., and Mu, J., 2021, "Recent Advances in Maturation of Pluripotent Stem Cell-Derived Cardiomyocytes Promoted by Mechanical Stretch," Med. Sci. Monitor, 27, p. e931063.

- [72] Lundy, S. D., Zhu, W.-Z., Regnier, M., and Laflamme, M. A., 2013, "Structural and Functional Maturation of Cardiomyocytes Derived From Human Pluripotent Stem Cells," Stem Cells Develop., 22(14), pp. 1991–2002.
 [73] Feinberg, A. W., Ripplinger, C. M., van der Meer, P., Sheehy, S. P., Domian, I.,
- Chien, K. R., and Parker, K. K., 2013, "Functional Differences in Engineered Myocardium From Embryonic Stem Cell-Derived Versus Neonatal Cardiomyocytes," Stem Cell Rep., 1(5), pp. 387–396.
 [74] Tulloch, N. L., Muskheli, V., Razumova, M. V., Korte, F. S., Regnier, M., Hauch,
- K. D., Pabon, L., Reinecke, H., and Murry, C. E., 2011, "Growth of Engineered Human Myocardium With Mechanical Loading and Vascular Co-Culture," Circ. Res., 109(1), pp. 47-59.
- [75] Ronaldson-Bouchard, K., Ma, S. P., Yeager, K., Chen, T., Song, L., Sirabella, D., Morikawa, K., et al., 2018, "Advanced Maturation of Human Cardiac Tissue Grown From Pluripotent Stem Cells," Nature, 556(7700), pp. 239-243.
- [76] Wang, J., Cui, C., Nan, H., Yu, Y., Xiao, Y., Poon, E., and Yang, G., 2017, "Graphene Sheet-Induced Global Maturation of Cardiomyocytes Derived From Human Induced
- Pluripotent Stem Cells," ACS Appl. Mater. Interfaces., 9(31), pp. 25929–25940.

 [77] Tu, C., and Zoldan, J., 2018, "Moving iPSC-Derived Cardiomyocytes Forward to Treat Myocardial Infarction," Cell Stem Cell, 23(3), pp. 322–323.

- [78] Esmaeili, H., Patino-Guerrero, A., Hasany, M., Ansari, M. O., Memic, A., Dolatshahi-Pirouz, A., and Nikkhah, M., 2022, "Electroconductive Biomaterials for Cardiac Tissue Engineering," Acta Biomater, 139, pp. 118–140.

 Vasquez, C., and Morley, G. E., 2012, "The Origin and Arrhythmogenic Potential of Fibroblasts in Cardiac Disease," J. Cardiovasc. Transl. Res., 5(6), pp. 760–767.
- [80] Ji, J., Ren, X., Gomez, J., Bashar, M. K., Shukla, N., Datta, S., and Zorlutuna, P., 2023, "Large-Scale Cardiac Muscle Cell-Based Coupled Oscillator Network for Vertex Coloring Problem," Adv. Intell. Syst., 5(5).
- [81] Ren, X., Gomez, J., Bashar, M. K., Ji, J., Can, U. I., Chang, H.-C., Shukla, N., Datta, S., and Zorlutuna, P., 2021, "Cardiac Muscle Cell-Based Coupled Oscillator Network for Collective Computing," Adv. Intell. Syst., 3(4), p. 2000253.
- [82] Shi, X., Qin, L., Zhang, X., He, K., Xiong, C., Fang, J., Fang, X., and Zhang, Y., 2011, "Elasticity of Cardiac Cells on the Polymer Substrates With Different Stiffness: An Atomic Force Microscopy Study," Phys. Chem. Chem. Phys., 13(16), pp. 7540-7545.
- [83] Gheorghe, A. G., Fuchs, A., Jacobsen, C., Kofoed, K. F., Møgelvang, R., Lynnerup, N., and Banner, J., 2019, "Cardiac Left Ventricular Myocardial Tissue Density, Evaluated by Computed Tomography and Autopsy," BMC Med Imaging, 19(1), p. 29.